Field comparison of network Sun photometers

L. J. Bruce McArthur,[1] David H. Halliwell,[2] Ormanda J. Niebergall,[2] Norm T. O'Neill,[3] James R. Slusser,[4] and Christoph Wehrli[5]

[1] Measurements of aerosol optical depth have become more numerous since the mid-1990s with the onset of commercially available, high-quality, low-maintenance automatic instrumentation. The development of several networks for aerosol measurements, and the next day availability of preliminary data for some, have further enhanced interest in the products this type of measurement can provide. With several networks operating globally and others operating either regionally or continentally within North America the comparability of the data emanating from the various archive centers is an important issue. The Bratt's Lake Observatory operates four separate types of Sun photometers in conjunction with three different networks: Aerosols in Canada, Global Atmosphere Watch, and the U.S. Department of Agriculture UV-B Monitoring Program. Data collected during the summer of 2001, following the protocols established by the networks and the Meteorological Service of Canada, were analyzed to determine the comparability among these networks. As the instruments and conversion algorithms are similar to other networks from around the globe, it is believed that the results of this comparison can be transferred, at least in part, to other operational networks. The results of the 3-month study indicate that the data obtained from the networks that operate direct-pointing instruments are very comparable, being within ±0.01 of an optical depth for instantaneous measurements during cloud-free line-of-sight conditions. Over the length of the comparison the root mean square difference of aerosol optical depth at 500 nm between the direct sun-pointing instruments was 0.0069. The rotating shadowband instruments did not perform as well. These results indicate that the data from well-maintained networks of direct sun-pointing photometers can provide data of the quality necessary to compare stations from across the globe. *INDEX TERMS:* 0305 Atmospheric Composition and Structure: Aerosols and particles (0345, 4801); 0360 Atmospheric Composition and Structure: Transmission and scattering of radiation; 0394 Atmospheric Composition and Structure: Instruments and techniques; 1640 Global Change: Remote sensing; 3359 Meteorology and Atmospheric Dynamics: Radiative processes; *KEYWORDS:* Sun photometer, AOD, Ångström coefficient

Citation: McArthur, L. J. B., D. H. Halliwell, O. J. Niebergall, N. T. O'Neill, J. R. Slusser, and C. Wehrli, Field comparison of network Sun photometers, *J. Geophys. Res.*, *108*(D19), 4596, doi:10.1029/2002JD002964, 2003.

1. Introduction

[2] Optical depth measurements are regularly acquired using Sun photometers or shadowband radiometers from a number of networks around the world. These measurements are used to provide global aerosol climatologies [*Holben et al.*, 2001; *Michalsky et al.*, 2001] and to validate satellite

aerosol observations on the one hand and provide atmospheric corrections for satellite retrievals on the other [*Fedosejevs et al.*, 2000]. Probably the best known of these networks is the Aerosol Robotic Network (AERONET) [*Holben et al.*, 1998], a NASA-operated network that employs the Cimel Sun photometer. The Canadian component of this network is Aerosols in Canada (AEROCAN) [*Bokoye et al.*, 2001]. The Global Atmosphere Watch Programme is presently equipping a number of its background sites with Precision Filter Radiometers (PFRs), designed and manufactured at Physikalisch-Meteorologisches Observatorium/World Radiation Centre (PMOD/WRC) (Davos, Switzerland) as part of the Swiss contribution to the World Meteorological Organization. Also capable of providing aerosol optical depth measurements within the continental United States (including two Canadian stations) is the U.S. Department of Agriculture (USDA) UV-B Monitoring Program using Yankee Environmental Systems (YES) Multifilter Rotating Shadowband Radio-

[1]National Atmospheric Radiation Centre, Meteorological Service of Canada, Toronto, Ontario, Canada.

[2]Bratt's Lake Observatory, Meteorological Service of Canada, Wilcox, Saskatchewan, Canada.

[3]Le Centre d'applications et de recherches en télédétection, Université de Sherbrooke, Sherbrooke, Canada.

[4]U.S. Department of Agriculture UV-B Monitoring and Research Program, Colorado State University, Fort Collins, Colorado, USA.

[5]Physikalisch-Meteorologisches Observatorium/World Radiation Centre, Davos, Switzerland.

meter (MFRSR) in both the UV and visible portions of the spectrum. These instruments are operated by the Natural Resource Ecology Laboratory (Colorado State University) [*Bigelow et al.*, 1998]. A second regional network operating MFRSR instruments in the United States is the Quantitative Links program [*Michalsky et al.*, 2001]. Further examples of regional networks are the Swiss national network [*Ingold et al.*, 2001], which uses a sun-pointing photometer, the Australian combined networks composed of 16 Australian Bureau of Meteorology stations that operate Carter-Scott SP01A and SP02 sun-pointing photometers, and three stations of the Commonwealth Scientific and Industrial Research Organisation Aerosol Ground Station Network that use the Cimel CE318 sun/sky photometer [*Mitchell and Forgan*, 2003].

[3] With the ever-increasing use of the World Wide Web as a means of propagating data quickly, results from a number of networks are now available within hours of the observations being made. This rapid publication of data encourages users from various disciplines to create value-added products by combining observations from various networks. Therefore it is important to know if the various products distributed in near-real-time, whether they be aerosol optical depth (AOD) or a parameter calculated from AOD, such as Ångström's coefficients, are comparable.

[4] The most commonly defined forms of AOD are based on the Beer-Lambert law for monochromatic radiation and are expressed, depending on the complexity of the air mass terms used, by

$$\delta_a = \ln(I_0/I)m^{-1} - \sum_i \tau_i \qquad (1)$$

or

$$\delta_a = \left[\ln(I_0/I) - \sum_i \tau_i m_i\right] m_a^{-1}, \qquad (2)$$

where for a given wavelength (λ), the AOD (δ_a) is a function of the monochromatic spectral flux measured at the surface (I), the extraterrestrial monochromatic flux (I_0) corrected for the sun-earth distance, the optical air mass (m), and the optical depth of the various atmospheric constituents (δ_i) that affect the transmission through the atmosphere such as molecular scattering and gaseous absorption. The major difference between the two methods is in the description of the vertical structure of atmospheric constituents. Equation (1), which is more commonly used, assumes that all constituents are vertically distributed in the same manner, while equation (2) recognizes that aerosols and atmospheric gases can be better modeled using individual scale-height air mass values (m_i).

[5] The formulation in the optical domain of Ångström's [1929] relationship, which is based on the simplest form of the aerosol size distribution for particles between ∼0.08 μm and ∼2 μm, is the Junge power law (r − γ) expression [*Junge*, 1963], between optical depth and wavelength

$$\delta_\lambda = \beta(\lambda/\lambda_0)^{-\alpha}, \qquad (3)$$

where δ_λ is the aerosol optical depth at wavelength λ (in μm), λ_0 is defined as the 1-μm wavelength. The parameter α is the

log-log slope of the curve (γ - 2) and is sensitive to the aerosol size distribution; as α increases, the number of small particles increases. The parameter β is the optical depth at a wavelength of 1 μm and is proportional to the vertically integrated aerosol concentration.

[6] Historically, instrument comparisons have consisted of bringing a number of instruments together to a single location for a period of several days to several weeks [e.g., *Schmid et al.*, 1999]. These types of comparisons are essential to moving forward the frontiers of instrument science. However, there may be little or no relation between the results of these intensive comparisons and the results from the same instruments when placed in an operational network setting. The comparison that is being reported on provides insight into the quality of data output by instruments when cared for following operational protocols designed by the various network investigators. Furthermore, the data that are compared comprise the normal product associated with the various data centers responsible for the routine handling of the measurements. Therefore the results of this comparison should provide an understanding both of the comparability between networks and of the overall data quality of the networks represented.

2. Comparison Locale

[7] The AERONET, Global Atmosphere Watch (GAW), and USDA networks intersect at the Bratt's Lake Observatory (BLO) (50°17′N, 104°42′W), a Baseline Surface Radiation Network (BSRN) station in the southern Canadian prairies. In addition to these network observations the observatory derives optical depths from a Meteorological Service of Canada (MSC) YES visible MFRSR and a pair of Middleton SP01A Sun photometers, similar to those used by the Australian Bureau of Meteorology in the combined Australian networks. The inclusion of the GAW PFR photometer in late spring 2001 provided the opportunity to compare the output of each of these different types of instruments over a longer period of time than the more normal high-intensity, short-duration, multinational comparison.

[8] The BLO is located in the southern Canadian prairies ∼60 km north of the Canada-U.S. border and 25 km south of Regina, Saskatchewan. Geographically, the area is extremely flat with the primary activity being low-intensity agriculture, primarily wheat. The climate is continental, the normal mean summertime temperature being ∼18°C. Convective cloud occurs most days throughout the summer, but precipitation is low. The summer of 2001 was particularly dry, and, consequently, the influence of windblown particulates exceeded normal levels. There are no significant local sources of anthropogenic air pollution, so aerosol optical depths are normally low [*Fedosejevs et al.*, 2000], although they peak during the summer period. Low aerosol optical depths present particular problems with network configurations where assumptions are made concerning pressure and absorbing gases.

[9] While measurements of many radiation, meteorological, and air quality variables are made at the observatory, two that significantly impact on the reduction of Sun photometer voltages to aerosol optical depth are air pressure and ozone amount. The local surface pressure is measured once per second with a 1-min average recorded. Because
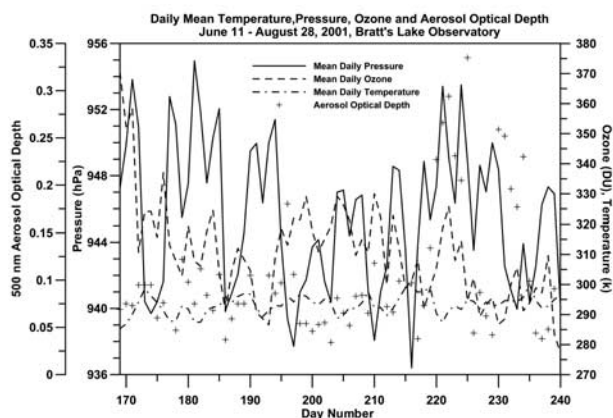
Figure 1. Variation in meteorological variables during the comparison. Daily temperature, pressure, ozone amount, and 500-nm aerosol optical depth (Aerosol Robotic Network (AERONET) Cimel).

pressure can vary significantly throughout the day and Rayleigh scatter is significant at short wavelengths when the optical depth is small, the coinciding pressure was used in the calculation of Rayleigh optical depth for the GAW instrumentation. Columnar ozone is measured up to 40 times per day using a Brewer Mk IV spectrophotometer [*Kerr and McElroy*, 1993] based on the ozone absorption coefficients of *Bass and Paur* [1985]. For the purposes of this comparison the daily mean column ozone was used to calculate the value of ozone absorption. Figure 1 shows the variation in mean daily temperature, pressure, ozone, and 500-nm aerosol optical depth, as determined from the Cimel Sun photometer data, for the comparison period.

3. Instrumentation and Network Protocols

[10] This section will briefly describe the network, the instrumentation used in the network, the protocols associated with the maintenance of the equipment, and the algorithms associated with the reduction of the electrical signal to aerosol optical depth, including any screening the network uses to quality assure the data with respect to interference from clouds. Table 1 provides a brief overview of each of the instruments, including pertinent facts associated with the collection and analysis of the data.

3.1. AEROCAN

[11] AEROCAN [*Boyoke et al.*, 2001] is the Canadian subset of the NASA AERONET federation of Sun photometer networks [*Holben et al.*, 1998] and consists of stations mostly in southern Canada. As part of AERONET, Cimel Sun photometers are used exclusively, and the network protocols set out by AERONET (available at http://aeronet.gsfc.nasa.gov/ (under "Operations")) are followed with respect to maintenance. The Cimel Electronique 318A photometer is a dual collimator instrument for the measurement of direct solar and sky radiances. The direct sun mode is measured using a solar collimator with a 1.2° field of view. Sky mode observations are made using a similar collimator with the incorporation of lenses to increase the signal. The instrument contains eight ion-assisted deposition

interference filters housed in a rotating wheel. The direct beam signal is measured with a UV-enhanced silicon photodiode. Corrections for photodiode and filter temperature dependencies are made based on an internal temperature sensor. The optical assembly is attached to a robot arm that uses a four-quadrant sensor to point the instrument with an accuracy of 0.1°. Further details on the filter configuration are in Table 1, and a more complete description is given by *Holben et al.* [1998]. The Sun photometer is routinely calibrated by shipping the instrument to NASA Goddard, where outdoor comparisons are made with a group of standard Cimel Sun photometers that are calibrated at Mauna Loa, Hawaii. The collected data are transmitted directly to AERONET, where automatic quality assurance is performed, including cloud screening [*Smirnov et al.*, 2000]. Part of this quality assurance procedure determines the data collection and data transmission offsets for individual instruments to within 1 s. Data are classified by level depending upon the quality assurance processing performed. Level 1.0 data has the preinstallation calibration coefficients applied to the data. Data that have been automatically cloud screened is classified as level 1.5 and are available from the AERONET Web site usually the day following the measurements. A higher-quality data product that incorporates a calibration stability check is available following the recalibration of the Cimel instrument (level 2.0). The Cimel instrument used for this comparison was calibrated immediately before the comparison period. Because of a mechanical failure in the instrument, the comparison was terminated and the instrument returned to NASA Goddard for repair and a postcomparison calibration. All three levels of data were used in this comparison. Levels 1.0 and 1.5 were employed in determining cloud-screening statistics, while the level 2.0 data were used for the AOD comparison. In this particular comparison, differences in AOD between the level 1.5 and level 2.0 data were insignificant.

[12] Although the Cimel is capable of measuring many more parameters than the direct beam spectral extinction, these are not considered in this comparison. Level 1.0 extinction data is observed once every 15 min and recorded only if the signal does not indicate severe cloud-induced instability (coarse precloud screening triplet rejection) or if precipitation is occurring. Subsequent level 1.5 cloud-screening criteria include a triplet check (temporal stability of three optical depth measurements) and a second-order temporal derivative constraint [*Smirnov et al.*, 2000]. As this is the most infrequent measurement of aerosol optical depth, the data from the other instruments involved in the comparison will be presented initially at this temporal interval.

[13] The remote nature of many of the AERONET locations has required that both the surface pressure (needed for the calculation of Rayleigh optical depth) and the columnar ozone amount (needed to calculate ozone absorption in the Chappuis band) be estimated. The former is based upon surface elevation and the standard atmosphere, while the latter uses a 5° gridded ozone climatology based on the work of *London et al.* [1976]. The determination of Rayleigh optical depth follows *Bucholtz* [1995], and the ozone absorption coefficients used are from *Vigroux* [1953]. *Eck et al.* [1999] give the maximum uncertainties

Table 1. Description of Network Photometers/Radiometers That Participated in the Network Comparison of Aerosol Optical Depth

Instrument	Wavelengths, nm	Method of Calibration	Method of Measurement	Sampling Rate	O₃ Amount	Atmospheric Pressure	Cloud Screening	Reference
AEROCAN Cimel	340, 379, 437, 498, 669, 871, 1021; full width at half maximum (FWHM) 10 nm	comparison with standard instrument	direct Sun, active tracking; filter wheel, single detector; field of view (FOV) 1.2°	Observation time, 8 s; sampling frequency, variable, dependent upon day length	tabular; 5° lat. and long. climatology	based on site elevation; 586.7 m	*Smirnov et al.* [2000]	*Bokoye et al.* [2001] and *Holben et al.* [1998]
GAW PFR	367.8, 411.9, 500.4, 862.9; FWHM 3.8–5.4 nm	comparison with absolute spectral radiometer; refined Langley and ratio-Langley calibration	direct Sun, active tracking; multiple sensors; FOV 2.5°	once per minute	on-site Brewer column ozone measurement	on-board pressure transducer	combination of *Smirnov et al.* [2000] and *Harrison and Michalsky* [1994]	*Wehrli* [2000]
Middleton SP01A	368, 412, 502a, 502b, 675, 778, 812, 862; FWHM 5 nm	Langley calibration (equation (1))	direct Sun, active tracking; multiple detectors; FOV 2.4°	once per minute	on-site Brewer column ozone measurement	local mean daily pressure	modified *Harrison and Michalsky* [1994]	*Harrison et al.* [1994] and *Bigelow et al.* [1998]
USDA MFRSR (Yankee Environmental Systems, Inc.)	415, 500, 610, 665, 860, 940; FWHM 10 nm	on-site progressive Langley calibration (equation (1))	residual calculation from global and diffuse irradiance measurements; multiple detectors; equivalent FOV	20 s averaged over 3 min	300 Dobson units	based on site elevation; 586.7 m	none	*Harrison et al.* [1994] and *Bigelow et al.* [1998]
MSC MFRSR	415.8, 496.4, 613.6, 671.6, 869.5, 937.5; FWHM 10 nm	on-site Langley calibration (equation (1))	residual calculation from global and diffuse irradiance measurements; multiple detectors; equivalent FOV	15 s averaged over 1 min	on-site Brewer column ozone measurement	local mean daily pressure	none	*Harrison et al.* [1994]

associated with these assumptions as equivalent optical depths. For a 3% difference between measured pressure and the AERONET static pressure calculation, the Rayleigh error was found to be ~0.021 at 380 nm, decreasing to 0.007 at 440 nm. Departures from the climatological mean ozone amount by 50% alter the aerosol optical depths by ~0.0036, 0.0045, and 0.0063 at 340, 500, and 675 nm, respectively. Overall, *Eck et al.* [1999] estimate the total uncertainty for network instrument measurements of AOD to be ~0.010–0.021, with the uncertainty increasing with decreasing wavelength.

3.2. U.S. Department of Agriculture UV-B Monitoring Program

[14] The USDA Ultraviolet Radiation Monitoring Program [*Bigelow et al.*, 1998] (available at http://uvb.nrel. colostate.edu/UVB/home_page.html) was developed primarily for the monitoring of spectral and broadband UV-B and UV-A, especially in rural areas, to determine their effect on agriculture. The primary instrument used is the YES MFRSR [*Michalsky et al.*, 1988; *Harrison et al.*, 1994]. These instruments are capable of measuring both the diffuse and global components of the incoming irradiance. Correcting for the directional variability associated with the nominally Lambertian (angularily independent) light-receiving diffuser head and knowing the solar zenith angle, the normal incidence direct beam irradiance can be calculated by subtracting the shadowed irradiance component from the total irradiance component. The USDA program uses two MFRSR instruments at each of its stations: one to measure the UV-B and UV-A at seven spectral wavelengths and another to measure the visible and near-infrared at six spectral wavelengths. A seventh channel in the visible light spectrometer/near-infrared (VIS/NIR) instrument measures a broader bandwidth that straddles the visible and NIR. This comparison uses only the VIS/NIR measurements. Light is transmitted to matched pairs of ion-assisted deposition interference filters and photodiode detectors through a Spectralon™ diffuser head. The entire detector canister is temperature controlled. Table 1 provides information on the wavelengths, bandwidths, and nominal field of view of the instrument.

[15] The measurement program uses a 20-s sampling period to obtain 3-min average values associated with the global and diffuse spectral irradiance. A single observation set consists of a global measurement on the time stamp and a corresponding diffuse observation ~7 s later. This delay in the determination of the direct beam is minor except during highly variable cloud conditions and can be equated to an air mass error of ~0.01 at air mass 6. The data are downloaded from the on-site data acquisition system on a daily basis, at which time the instrument clock is checked and maintained to within ±4-s accuracy. The 3-min average values are then used to calculate the average normal incidence direct beam spectral irradiance using the mean solar zenith angle for the sampling period. (This sampling period is greater than reported by *Bigelow et al.* [1998] because of the more northerly location of the instruments.) Maintenance consists of ensuring that the diffuser is clean of debris and the shadowband is correctly shading the diffuser. The instrument is monitored remotely on a daily basis and inspected biannually by technicians from the network. On-site personnel correct problems associated with the instrument between visits. The data is downloaded and processed daily.

[16] Calculation of the AOD is based on the mean voltage associated with the calculated direct measurement. The wavelength-dependent top-of-the-atmosphere coefficients for the instrument are calculated from a linear regression of daily Langley calibrations obtained on-site using the objective algorithm of *Harrison and Michalsky* [1994]. This method is similar to that of *Michalsky et al.* [2001]. In a fashion similar to AERONET, the USDA assumes a constant surface pressure based on elevations. Rayleigh optical depths are then calculated using the parameterization of *Stephens* [1994]. Ozone amount is set at a constant value of 300 Dobson units (DU). Using the ozone absorption coefficients of *Shettle and Anderson* [1995], the uncertainty in the AOD at 610 nm is calculated to be ~0.01 for a 75-DU error in ozone amount.

3.3. Global Atmosphere Watch Precision Filter Radiometer Network

[17] The primary purpose of the GAW Sun photometer network is to measure small changes in the global background aerosol. Stations are generally located in pristine locations where aerosol optical depths are small. The instrument, developed at the World Radiation Center Physikalisch-Meteorologisches Observatorium Davos (WRC/PMOD), is designed to provide precise optical depth measurements over long periods without changes in the instrument character. An example of the care in designing such a background network is the purchase of all of the interference filters for present and future instruments from the same filter lot so the intercomparability between instruments would be maintained. The instrument uses four independent silicon photodiode detectors offset by 3° from the optical axis in order to reduce interreflections between the detector and the light transmitted through the ion-assisted deposition interference filters. To eliminate temperature dependencies and reduce degradation, a Peltier-type thermostatic control is used to maintain a constant temperature of 20.5°C ± 0.1° throughout the instrument's operating range. The optical components are housed in an airtight tube that is slightly overpressured with dry nitrogen. For further protection the filters are shuttered from the Sun between the once per minute observations. The instrument's field of view is 2.5°. Table 1 provides filter information. A pressure transducer is included in the control unit to provide accurate observations for the calculation of Rayleigh optical depths. Unlike the AERONET Cimel that has a pointing robot as an integral part of the instrument, the GAW PFR must be pointed using a separate device. To monitor the quality of the external pointing, the photometer has a built-in quadrant detector with a range of ±0.75° in both axes.

[18] The instrument is calibrated using a combination of methods, including absolute calibrations traceable to Physikalisch-Technische Bundesanstalt Berlin (Germany) [*Wehrli*, 2000], Langley calibrations and comparison measurements at the World Radiation Centre, and Langley and ratio-Langley [*Forgan*, 1988] calibrations at the BLO. The Langley calibration uses equation (2) (refined Langley) to better estimate the actual structure of individual atmospheric components. The instrument was installed at the

Observatory in April 2001 and was, in part, the impetus for performing a comparison of this nature.

[19] The maintenance procedures for the PFR instrument include cleaning the outer quartz window each day as well as after precipitation events and ensuring that the data collection time is correct and the tracker on which the instrument is mounted is operating correctly. At the observatory the instrument is mounted on a Kipp and Zonen 2AP with active eye tracking. The data are collected by a Campbell Scientific CR10 datalogger that is interrogated every 6 hours, at which time the clock is checked and corrected to within 1 s. Each night, this data is downloaded to the Meteorological Service of Canada facility in Toronto via the Internet and then placed on an ftp server to be collected by the WRC/PMOD.

[20] Observations used in the present study were processed and quality assured in Toronto using the software designed by the WRC/PMOD for processing all GAW network data. Rayleigh optical depths are calculated using the observed pressure, the Rayleigh coefficients of *Bodhaine et al.* [1999], and the air mass calculations of *Kasten and Young* [1989]. Ozone optical depths are calculated on the basis of the mean daily columnar ozone amount as measured by the MSC Brewer Spectrophotometer [*Kerr and McElroy*, 1993] using the absorption coefficients obtained from the Simple Model of the Atmospheric Radiative Transfer of Sunshine 2 (SMARTS2) spectral model [*Gueymard*, 1995] and the *Komhyr* [1980] correction for the ozone air mass. Aerosol optical depth is calculated on the basis of the water vapor air mass calculation of *Kasten* [1966]. The data are screened and flagged for instrument temperature and pointing errors and checked for cloud contamination. The first gross check is the removal of all aerosol optical depths >2.0. Two more sophisticated, objective algorithms are then employed: an objective algorithm similar to that of *Harrison and Michalsky* [1994] and a triplet comparison method to remove thin cloud.

3.4. Meteorological Service of Canada Instruments

[21] Observations of AOD are obtained by both a YES MFRSR instrument and Middleton SP01A Sun photometers. Both are controlled through the BLO local area network by which the appropriate clock settings are maintained to better than 1 ms by a precision GPS time card installed in the central server (TrueTime, Time Traveller 32). The MFRSR is similar to the USDA instrument that measures in the visible portion of the spectrum. Differences in the sampling rate and the actual spectral characteristics of the interference filters are provided in Table 1. Maintenance is also similar for the two instruments with the exception that the USDA instrument is inspected twice yearly by their own technicians. Data are collected using the same type of data acquisition system and downloaded for processing at the observatory. Ongoing calibration of the instrument based on half-day Langley analyses in a manner similar to that of the USDA is performed. The cosine response function of the diffuser is that provided by the manufacturer. A cloud-screening procedure had not been implemented at the time of the comparison, so data were eliminated as having cloud interference using the times associated with cloud-contaminated data of the GAW PFR.

[22] The Middleton SP01A Sun photometer is a temperature-controlled four-wavelength instrument that employs a moving shutter to measure both the direct solar signal with a field of view of 2.4° and the solar aureole between 3° and 5° by blocking the center portion of the opening aperture. When not making observations, the shutter is closed to reduce solar degradation of the interference filters. To increase the number of spectral observations, a two-photometer system is employed where each instrument contains a 500-nm filter to ensure that the photometers are both correctly coaligned and operating in tandem, plus three other wavelengths (see Table 1). Data are eliminated when the difference in optical depth between the two 500-nm filters is >0.005. Both photometers are mounted on the same tracker and pointed using their respective diopters. Active tracking is accomplished using a quadrant sensor with a pointing accuracy of 0.1°. Both instruments and the tracker are controlled by unified software developed by the Australian Bureau of Meteorology for Middleton Instruments. Observations are made once per minute throughout the daylight period. Maintenance consists of cleaning the quartz glass covering the apertures, ensuring the correct time, and checking that the diopter sightings have not been altered accidentally. Calibration of the instrument is based on a combination of biennial Langley calibrations performed at Mauna Loa, Hawaii, and ongoing Langley analyses between calibration trips. A comparison of Langley calibration results between those obtained at Mauna Loa during March and April 2000 and those closest to the time of the comparison indicated no significant change in the responsivity based on the Langley-to-Langley variability at the BLO. The aerosol optical depths calculated during the comparison period are based on the Mauna Loa Langley analyses. During routine maintenance of the instrument in March 2002, filter transmission functions measured using a Perkin Elmer Lamda 9 spectrometer were compared with those measured using the same instrument in March 2000. With the exceptions of the 778-nm filter (peak transmittance changed from 56.35% in 2000 to 57.25% in 2002) and the 862-nm filter (peak transmittance increased to 71.9% from a 2000 value of 70.4%), the transmittance values were measured to within 0.1% of the 2000 value. The peak wavelengths were found to have remained unchanged within the instrumental resolution.

[23] The calculation of Rayleigh optical depth is based on mean daily pressure and coefficients based on the work of *Chance and Spurr* [1997]. Ozone optical depth is calculated using the mean daily columnar ozone amount and the absorption coefficients for a temperature of −40°C [*Burrows et al.*, 1999]. All air mass calculations for this study were based on the work of *Kasten and Young* [1989]. This differs significantly from the Australian networks that use component air mass values as a means of better estimating the very low aerosol optical depth values of Australia [*Mitchell and Forgan*, 2003].

[24] A cloud-screening procedure is applied to each half day of data based on the sum of the eight-channel voltages for each minute. The two stages of the process are similar to the methods outlined by *Harrison and Michalsky* [1994]. In the first stage the change in voltage is tracked from large to small air mass to detect decreases in voltage. Any decrease beyond a threshold voltage value is assumed to mark the

beginning of a cloud passage. The screening process detects a decrease whether it occurs in a single minute (i.e., between successive readings) or over several minutes. Once cloud has been detected, periods continue to be marked as cloudy until the value of the voltage increases above the precloud maximum. The voltage used in the process is the sum of all channel voltages. This is combined with the requirement that decreases in the summed voltage must be larger than a threshold value so that minor variations in optical depth or variations due to measurement noise are less likely to be treated as cloud

$$\left(\sum_{k=j-l}^{j-1} \Delta V_k \right) + \Delta V_j \leq 0 \Rightarrow \text{Cloudflag(True)}, \qquad (4)$$

where

$$\Delta V_j \equiv \left[\left(\sum_{i=1}^{8} V_i \right)_{j+1} - \left(\sum_{i=1}^{8} V_i \right)_j \right] \leq -V_{\text{Threshold}}, \qquad (5)$$

and the subscripts i, j, and k refer to the voltage of an individual channel, the total voltage associated with an individual observation, and the summation of voltages from the first flagged voltage (j-l) with decreasing air mass, respectively. The threshold voltage ($V_{\text{Threshold}}$) was set to 0.005 V compared to the sum of the extraterrestrial voltage (V_0) values for the eight channels of 14.0 V. The use of a summation of the eight channels also implicitly invokes a weighting on different wavelengths. The V_0 values range from 0.9 to 4.2 V and depend on both the extraterrestrial radiation value and the variable amplification for each channel in the instrument circuitry. Consequently, the greatest weighting tends to be on the 675-, 778-, and 812-nm wavelengths, with the absolute weight of individual channels varying with air mass.

[25] The second stage of the cloud-screening procedure takes the unscreened data from stage one and regresses log (voltage) against relative optical air mass (i.e., a Langley plot). Data found to be more than 3 standard errors from the regression line are flagged. After stage one cloud screening is complete, stage two rarely removes more than a few points.

4. Methodology

[26] The comparison is based on the AOD values provided by the individual networks. These values are calculated using the assumptions described in sections 3.1–3.3 for the determination of surface pressure and ozone amount, the selection of gaseous absorption coefficients, the method of calculating molecular scattering, and the use and method of calculation of single or multiple air mass values. Each of these components will affect the final optical depth calculations, with the differences between networks varying differently by wavelength and optical air mass. While a complete uncertainty analysis for each instrument and network would provide a means of quantitatively assessing the differences between observations, that is beyond the scope of this work. *Mitchell and Forgan* [2003], *Ingold et al.* [2001], *Eck et al.* [1999], and *Forgan* [1994] all provide

uncertainty analyses for instruments or methods of calculating AOD that are used in the present comparison. While each method of determining the uncertainty differs slightly from the others, a reasonable estimate of AOD uncertainty would be between 0.005 and 0.02 dependent on wavelength, instrument, and the procedure used in calculating the AOD.

[27] The comparisons presented consider both the temporal resolution of the data and whether or not the standardized algorithms used in the reduction of the output voltages into AOD use cloud screening. In some cases, where the cloud-screened data are flagged but not automatically removed, comparisons between instruments are done using combinations of the flagged and unflagged observations. During the course of the comparison, 12 half days were found to provide a significant number of observations that were influenced neither by cloud contamination nor by large changes in the AOD. These periods were used to calculate mean Ångström coefficients from the data collected by each of the instruments.

[28] As the observation schedule of the NASA Cimel was the least frequent of the instruments, it was decided that the first observational data set would be based on the Cimel observation times. The number of observations in the Cimel set are reduced from the nominal four times per hour by both the coarse triplet cloud screening made at the instrument and the automatic cloud screening associated with the calculation of level 1.5 and level 2.0 AOD data. The closest observation to each Cimel observation was selected for each of the instruments. For the PFR, SP01A, and MSC MFRSR instruments, measurements within 30 s of the Cimel observation were chosen, while observations within 90 s of the midpoint of the USDA MFRSR 3-min time average were selected. There were a number of occurrences when observations were not found within the appropriate time period, primarily due to routine maintenance or instrument malfunctions. In the case of the PFR data set, observations were flagged as unacceptable because the pointing-accuracy limit was exceeded or instrument temperature threshold was exceeded. In the case of the SP01A combination, data were flagged as unacceptable when the 500-nm AOD threshold was exceeded. Although the MSC MFRSR provides 1-min data, it is based on the average of the 15-s observations centered on the minute and is therefore a hybrid between the instantaneous measurements of the three direct-pointing instruments and the 3-min averaged data produced by the USDA MFRSR. Following the comparison of the observations on the nominal 15-min sampling rate of AERONET, a similar procedure was employed using the 1-min data of the GAW PFR and then the MSC SP01A instruments as the reference. Finally, the two MFRSR instruments are evaluated at the 3-min averaging times of the USDA network.

[29] A second difference between the observation schedule of the AERONET Cimel and the other instruments is that the former limits measurements to lower air mass values. Therefore, in the comparison of instrument pairs that do not include the Cimel, two sets of results are presented: one that includes all quality-assured data and another that limits the data to air mass values that do not exceed 6.

[30] The data reduction algorithms of the three direct-pointing instruments include automatic cloud-screening pro-

cedures. The GAW network and the MSC SP01A algorithms flag data as cloud contaminated, while AERONET removes the data from the published product entirely. Nevertheless, by using the level 1.0 (coarse instrument screening) and level 2.0 (final cloud screened) data from AERONET and the flagged data from the other two instruments, a comparison of the cloud screening procedures can be made. As there were no cloud observations made at the observatory, a definitive conclusion as to the quality of the cloud-screening procedures is not possible.

[31] In cases where both instruments determined whether an observation was cloud contaminated, results are presented first when only the reference instrument determines the line of sight is cloud-free and then when both AOD calculations indicate no cloud contamination. For those instrument pairs where only one cloud-screening algorithm was available the results are based on this data. As there is no cloud screening associated with either MFRSR instrument, the results have been filtered using the GAW PFR cloud-screened observation times. Even with the time stamp coordination and the combined cloud screening, a number of obvious outliers remained. If differences in the AOD at a given wavelength between two instruments was found to be >1.0, the observation pair was eliminated. This type of screening usually removed data during periods of consistent tracking problems associated with one of the instruments or when the solar intensity was low. A final filter used on each wavelength pair before comparison statistics were calculated was the removal of any data pair that was found to have an AOD difference >3 standard deviations from the overall mean AOD difference. This last filter normally removed very few observations, and those removed were found to be arbitrarily distributed throughout the observation period.

[32] The AERONET, GAW, and MSC algorithms provide routine calculations of the instantaneous Ångström Alpha exponents. Using the cloud-screened data sets, these are also compared during the entire period. For the AERONET data, which calculates Alpha based on both the complete wavelength range and the four wavelengths between 400 and 900 nm, the latter were used as to be comparable to the other instruments that do not measure at wavelengths >1000 nm. The Ångström Alpha coefficient is highly dependent on the overall shape of the aerosol size distribution [*O'Neill et al.*, 2001] and therefore the wavelengths chosen for its calculation [*Cachorro et al.*, 2001]. Nevertheless, most researchers using such data will probably not consider the type of aerosol or the manner in which the coefficient is calculated but will compare the exponents directly. Therefore, rather than rework the Alpha exponent algorithms for each instrument in order to arrive at a common set of computation wavelengths, the approach used was to compare the standard algorithmic outputs. Because this parameter is used so routinely, the variability of differences in the instantaneous values provides a rough measure of the uncertainty in the physical or optical properties inferred from the spectral behavior of the aerosol optical depth.

5 Results

5.1. Optical Depth

[33] The data used for the comparison of the five instruments were collected between 11 June and 28 August 2001

(days 162–240). The primary analysis compares the optical depths calculated using similar wavelengths between instruments. The filters in the two instruments having a 368-nm wavelength differ in central wavelength by only 0.2 nm. The range of central wavelengths in the visible portion of the spectrum among all instruments is within 6 nm. For the NIR region around 860 nm the difference between central wavelengths increases to 9 nm. The difference in central wavelengths in the visible portion of the spectrum is comparable to the estimated uncertainty quoted by filter manufacturers on stock filters. Aerosol optical depths, in general, vary slowly with wavelength so that slight changes in filter wavelengths should not significantly alter the overall results of the experiment. At shorter wavelengths the variation in Rayleigh optical depth is significantly greater than the variation in the AOD and therefore can be used as a means of conceptualizing the maximum difference that could be expected because of the discrepancy in the wavelength centers. The change in Rayleigh optical depth associated with the wavelength range about the 368-, 412-, and 500-nm filters is 0.0011, 0.0112, and 0.0062, respectively.

[34] Although the primary aim of this comparison was to better understand the application of network measurements to trend studies and the ability to develop a single global climatology from multiple networks without introducing network bias, a comparison of the daily progression of observations for each instrument was revealing. Figure 2 plots the 500-nm AOD for two periods and the 865-nm AOD for the second of these periods. The 6 and 7 July (day number 187 and 188) time period is for virtually cloudless conditions (Figure 2a), while the 26 August graph (day number 238) (Figure 2b) illustrates the cloud removal schemes associated with the PFR and SP01A instruments. For all instruments the AOD increases dramatically at larger zenith angles with the exception of the Cimel, which does not report data for air mass >5. Although the optical depths for each of these 3 days never exceeds 0.1 at zenith angles <80°, several typical characteristics of instrument behavior are apparent. Overall, the direct-pointing instruments track well, with the PFR normally reporting the largest optical depths and with the Cimel values being slightly less than the SP01A at 500 nm. The data on days 187 and 188 show the variability in the difference between the PFR and the Cimel and SP01A AOD diurnally and from day to day. On day 238, data from the Cimel and SP01A are stable or gradually declining AOD in the late morning (238.3–238.5) while the PFR data show a gradual increase. The Cimel data also show more variability through this period than the other two direct sun instruments, with the SP01A showing the lowest variability on day 238 (the variances being 8.7×10^{-5}, 6.2×10^{-5}, and 3.5×10^{-5} for the Cimel, PFR, and SP01A, respectively). Although the AOD is low between 238.45 and 238.65, the cloud-screening algorithms indicate significant cloud (lighter-colored, open symbols in Figure 2b for the PFR and SP01A, while periods during this time are absent for the AEROCAN Cimel data). Abrupt changes in the AOD at 238.65 indicate the onset of what is most probably cloud, but the earlier data may or may not indicate cloud contamination. The capabilities of cloud-screening algorithms are discussed in more detail in section 5.3.
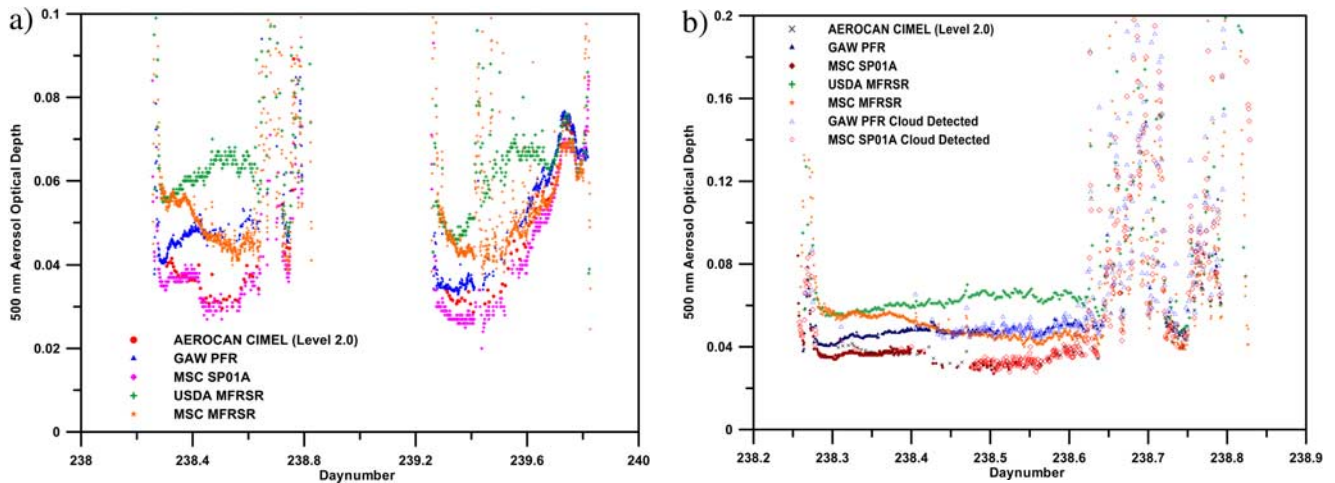
Figure 2. Aerosol optical depth at 500 nm as measured by the participating instruments: AERONET Cimel, Global Atmosphere Watch (GAW) Precision Filter Radiometer (PFR), Meteorological Service of Canada (MSC) SP01A, U.S. Department of Agriculture (USDA) Multifilter Rotating Shadowband Radiometer (MFRSR), and MSC MFRSR. (a) 6 and 7 July 2001. (b) 26 August 2001.

[35] Throughout the comparison period, the patterns for the two MFRSR instruments differ significantly from the direct beam instruments and each other in the manner illustrated in Figure 2. In the case of the USDA MFRSR the aerosol optical depths track reasonably well at larger zenith angles but deviate upward at high sun angles. This pattern is particularly interesting in that when calculating half-day Ångström coefficients using the AERONET air mass bounding protocol of values between 2 and 4 (see below), the discrepancy is excluded. *Schmid et al.*'s [1999] Figure 2 shows a similar type of behavior for the MFRSR 865-nm wavelength used in the fall 1997 Intensive Observation Period and *Mitchell and Forgan*'s [2003] Figure 7 illustrates the same pattern in a comparison with a Cimel 318A Sun photometer in Australia. The MSC MFRSR gives larger optical depths during the forenoon than the direct beam instruments, with the discrepancies lessening near noon and nearly replicating the direct beam photometers during the late afternoon. To determine if these patterns exist throughout the data set, Figure 3 plots the solar A.M. and P.M. differences of the AOD_{500} (GAW PFR-MFRSR) against air mass. The USDA (top panel of Figure 3) shows what appears to be the somewhat typical overestimation of AOD at low air mass and a moderate difference between A.M. and P.M. performance. The MSC MFRSR also has an A.M.-P.M. hysteresis but with a slight difference in the slope between the morning and afternoon. At approximately air mass 10 there is a significant change in the trend of the differences related to poorer performance at larger zenith angles. These results illustrate the sensitivity of the more complex MFRSR instruments to directional responsivity characterization.

[36] Figure 4 (the scales are identical for each panel for ease of comparison) plots the differences between comparable wavelengths (415, 500, 665, and 862 nm) of the MSC SP01A and the two MFRSR instruments for the complete cloud-screened (as determined by the MSC SP01A algorithm) data set against air mass <6 to show if there are any similarities between wavelengths. The differences between SP01A and PFR and SP01A and Cimel comparable wave-

lengths are also plotted and will be considered in detail below. Only those data pairs when both cloud-screening algorithms indicate a clear line of sight have been used in these latter comparisons. The general scatter of the MFRSR instruments is greater than for the Cimel or PFR instruments. This increased scatter is probably a function of the temporal averaging used for both MFRSR instruments, the variation of the instrument field of view with changing zenith angle, and the complexity of the conversion from global and diffuse spectral irradiance values to AOD. The plots also show the hysteresis about solar noon that is in evidence in Figure 3. The level of each instrument was checked throughout the comparison as part of the routine maintenance to ensure that the bubble levels were correct. Neither instrument was found to be out of level during the period of the comparison. This suggests that the optical head is not parallel to the base of the instrument on which
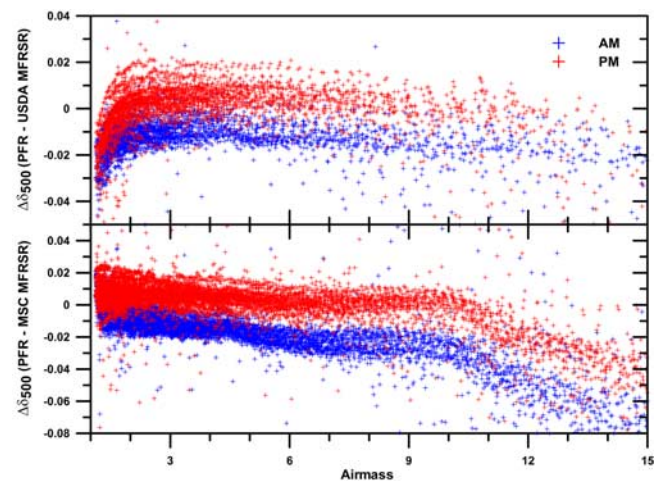
Figure 3. Variation of δ_{500} differences between the GAW PFR and the USDA and MSC MFRSR radiometers as a function of A.M. and P.M. air mass.
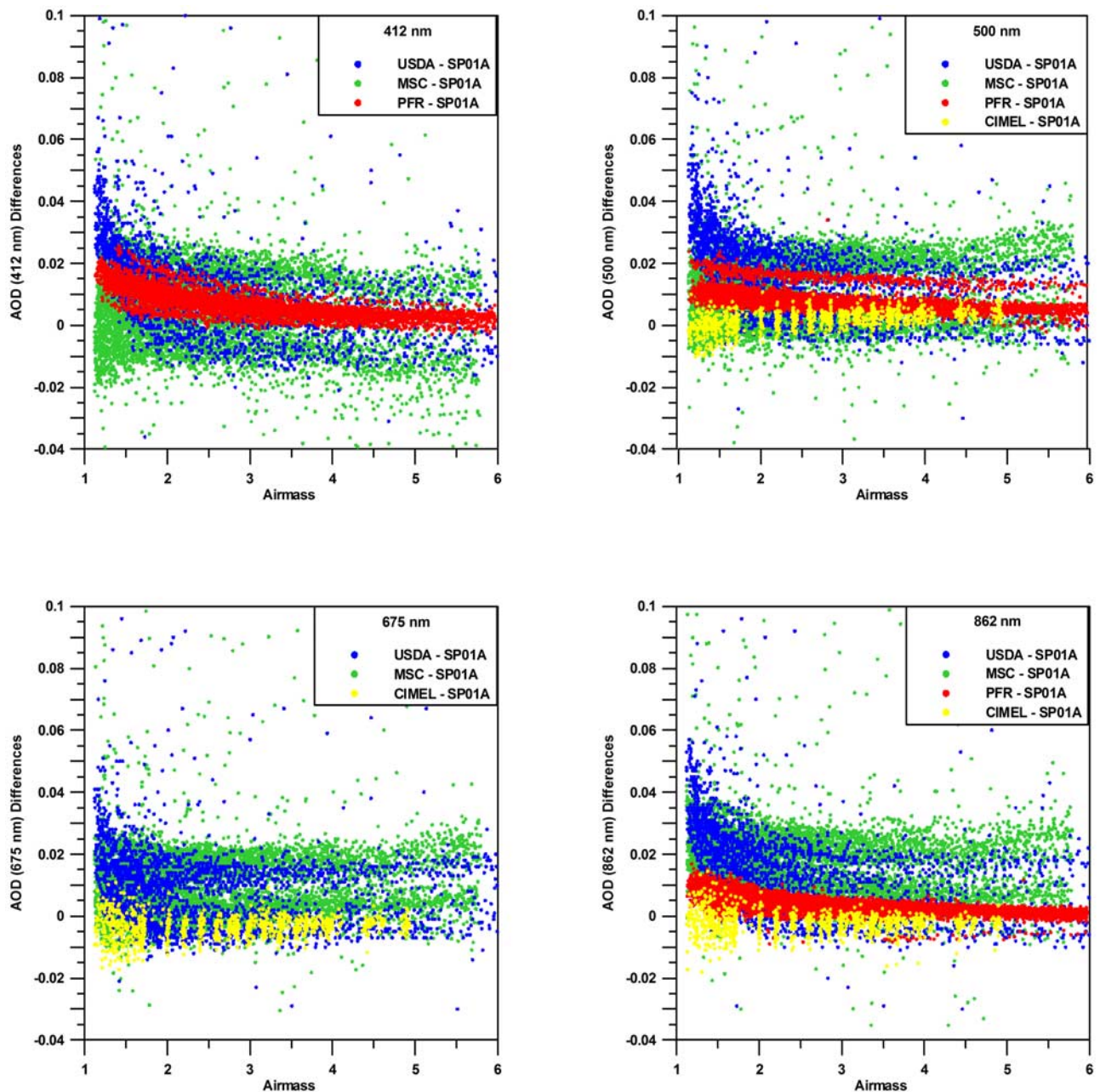
Figure 4.   The variation in aerosol optical depth (AOD) differences at four different USDA MFRSR wavelengths as a function of zenith angle. For comparison, comparable wavelengths of the GAW PFR and the AERONET Cimel are also plotted. The reference instrument for each pairing is the MSC SP01A.

the bubble level is attached. As both instruments were operational throughout the 2000–2001 winter, this may indicate that regular optical leveling of this type of instrument is necessary because differential expansion and contraction between the base and the optical assembly affects the overall radiometric alignment of the instrument. The placement of the level on the optical assembly of the instrument could also reduce this type of problem. Another problem associated with the MFRSR instruments is the deterioration of the Teflon™ diffuser due to natural soiling and deterioration by the elements. Neither of these MFRSR instruments has had an angular characterization since being acquired in the late 1990s. These results confirm that the

characterization of the angular response be done frequently (as suggested by the manufacturer) for these types of instruments if accurate determinations of AOD are required.

[37]   The increased differences between the SP01A and the USDA MFRSR at low air mass values, as observed in Figure 4, are a common phenomenon throughout the comparison. This is apparent for each wavelength but is especially large for 500 nm, reaching differences of >0.05 regularly, with the change in the curvature of the distribution occurring at approximately air mass 2. The 675-nm wavelength is the least affected. Noting the form of equations (1) and (2) (see Figure 6), the shape of the difference curves between the USDA MFRSR and the MSC SP01A
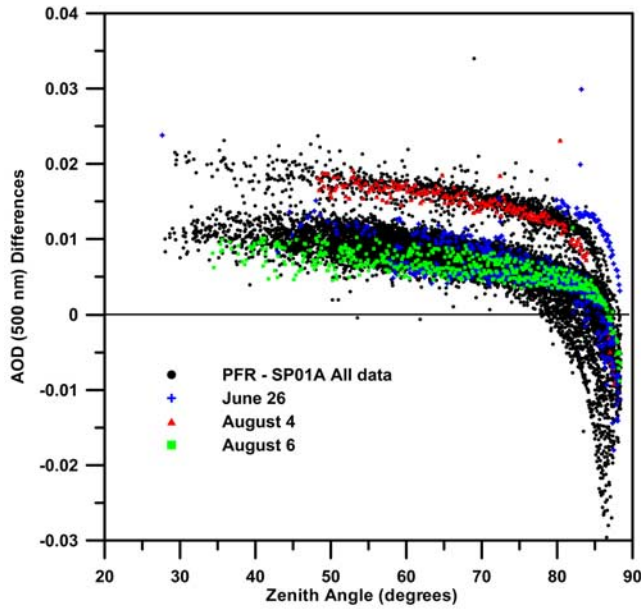
Figure 5. Variation in the 500-nm AOD differences between the GAW PFR and the MSC SP01A Sun photometers with zenith angle.

may be explained as an incorrect extraterrestrial constant (I_0) for one of the two instruments. This would increase the magnitude of the differences at small air mass values (that would vary as $(1/m)\, dI_0/I_0$ but becomes nearly asymptotic as air mass increases and other error sources become more predominant. The MSC MFRSR does not exhibit this pattern except for the 862-nm wavelength.

[38] Similar changes in trend are also evident between the SP01A and the PRF instruments for the 412- and 862-nm wavelengths and to a very small extent between the SP01A and the Cimel at the 862-nm wavelength. In combination with the changes in the transmission of the 862-nm filter noted earlier, it would suggest that the calibration coefficient used for the 862-nm filter of the MSC SP01A is suspect. The AOD differences between the SP01A and Cimel in Figure 4 show a slight change in slope in the 500-nm plot that is not found between the SP01A and the PFR. The use of a constant pressure term in the determination of Rayleigh optical depth and the use of climatological ozone optical depths yield error dependencies that resemble these small differences. To a lesser extent, differences in the ozone absorption coefficients used by each of the networks would also account for a small portion of the bias.

[39] The AOD differences between the GAW PFR and the MSC SP01A at 500 nm, and to a lesser extent at 412 nm, appear to split into two separate groups of points. This divergence, however, is not related to hysteresis about solar noon as it occurs as an offset, generally for part of or an entire day, returning to "normal" just as rapidly. Figure 5 illustrates these two families for the 500-nm AOD differences for the GAW PFR and MSC SP01A pairing. Superimposed on the entire data set are several individual days representative of these variations. This same pattern exists between the AERONET Cimel and the GAW PFR, indicating that the problem may be associated with the PFR. An obvious explanation would be errors associated with the

solar tracking, but examinations of the pointing signals recorded within the GAW PFR data records do not show significant differences between the days that exhibit larger AOD differences and those within the larger family of observations. It should be noted that GAW PFR observations that exceed the pointing criterion of 15 arc min were eliminated from the data before this analysis. These systematic differences cannot be explained at present.

[40] To quantitatively describe the relationship between the AOD for the wavelength pairs of the various instruments over the duration of the comparison, the root mean square difference (RMSD) and the mean bias difference (MBD) were computed. These can be considered as components of the sample variance (σ^2)

$$\sigma^2 \cong RMSD^2 - MBD^2, \tag{6}$$

where

$$RMSD = \left(N^{-1} \sum_1^N (obs_i - ref_i)^2 \right)^{0.5} \tag{7}$$

$$MBD = N^{-1} \sum_1^N (obs_i - ref_i). \tag{8}$$

The RMSD is often associated with the nonsystematic component of the differences, being sensitive to extreme values, while the MBD describes the offset between sets of observations. This methodology assumes a stationary distribution of differences, which would be expected if the method of calculating the AOD was the same for all networks and the extraterrestrial coefficients were correct. However, as observed from Figure 4, this is not the case for some of the instrument filter pairs. Therefore the results should be regarded as an estimate of the differences between AOD, especially between instrument pairs where one instrument calculates AOD using equation (1) and the other uses equation (2). Figure 6 illustrates some of the air mass dependencies on AOD when using these two calculation methods. The differences are based on a
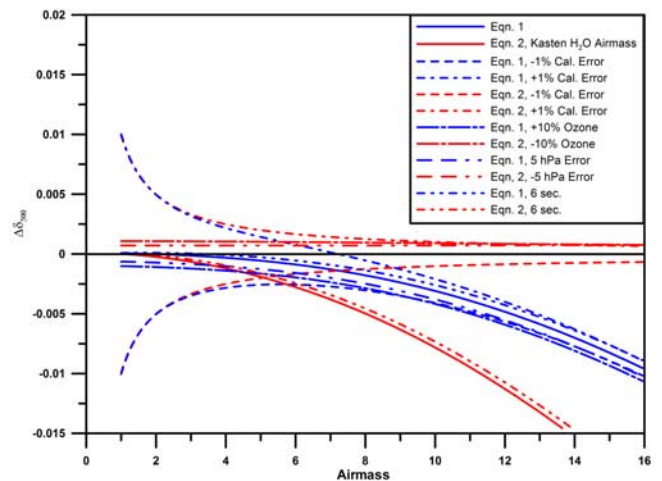
Figure 6. Examples of the magnitude of differences in AOD associated with differences in the method of calculation, uncertainties in instrument calibration, and incorrect estimates of atmospheric quantities.

Table 2. Mean Bias Difference, Root Mean Square Difference, and Standard Deviation Between Aerosol Optical Depths at Cimel Sun Photometer Wavelengths and the Corresponding Wavelengths of the Other Sun Photometers in the Comparison[a]

Instrument	Wavelength, nm	All Data MBD	All Data RMSD	All Data σ	N[b]	Clear MBD	Clear RMSD	Clear σ	N
GAW PFR	500.4	0.0095	0.0122	0.0076	1724	0.0068	0.0085	0.0055	998
	862.9	0.0083	0.0101	0.0057	1725	0.0064	0.0072	0.0035	998
MSC SP01A	502	−0.0008	0.0042	0.0041	1534	−0.0021	0.0036	0.0029	975
	675	0.0039	0.0059	0.0044	1539	0.0036	0.0049	0.0033	975
	862	0.0021	0.0050	0.0045	1518	0.0022	0.0039	0.0032	956
USDA MFRSR	500	0.0195	0.0257	0.0168	1835				
	665	0.0149	0.0200	0.0132	1835				
	860	0.0203	0.0255	0.0154	1834				
MSC MFRSR	496.4	0.0100	0.0178	0.0147	1837				
	671.6	0.0143	0.0208	0.0151	1837				
	869.5	0.0212	0.0252	0.0136	1835				

[a]MBD, mean bias difference; RMSD, root mean square difference; σ, standard deviation. Cimel Sun photometer wavelengths are 498, 669, and 871 nm.
[b]Sample size.

calculation of AOD using equation (2) with an assumed atmosphere having an aerosol layer with a 6.5-km scale height and an ozone layer with a 21-km scale height. The Rayleigh air mass function is calculated using the work of *Kasten and Young* [1989]. Calculations made using equations (1) and (2) differ from the original calculation only in the prescribed differences of incorrect instrument extraterrestrial coefficients (±1%), incorrectly prescribed atmospheric pressure (5 hPa), and incorrectly prescribed ozone (10%). The differences associated with an incorrect clock setting of 6 s are calculated for the time being fast for decreasing air mass on 21 June at BLO. For the comparison of equations, all equation (2) curves were calculated using the Kasten water vapor air mass for aerosol. The differences between the two equations using identical air pressure and ozone amount are shown as equation (1) in Figure 6. Differences in air pressure and ozone amount behave, to a first approximation, as simple biases on the AOD differences, while differences associated with the two methods of calculation increase with increasing air mass. It should be noted that the same asymptotic behavior exhibited in the use of an incorrect extraterrestrial coefficient using equation (2) would be exhibited using equation (1) if the original method of determining the AOD assumed a single air mass for all components.

[41] Tables 2–5 provide the MBD, RMSD, and sample size (N) for the various combinations of instruments and filters, beginning with the AERONET Cimel instrument as the reference. The PFR, MSC SP01A, and finally the USDA

MFRSR then follow as references. The wavelengths given in Tables 2–5 refer to the instrument that is being compared with the reference; the reference wavelengths are given in the caption. A negative MBD results when the AOD of the instrument that is being compared is less than the reference photometer AOD. The "All Data" heading (Tables 2–4) indicates that each quality assured observation, with the exception of cloud-flagged data from the GAW PFR and the MSC SP01A, were compared against the corresponding reference observation. The "Clear" designator in the column heading (Table 5) indicates that both the cloud-screening algorithm of the reference and the cloud-screening algorithm of the instrument being evaluated determined that no cloud was present in the line of sight to the sun. As no separate cloud-screening programs are associated with the MFRSR data, comparisons are based on the reference photometer cloud-screened data.

[42] The results are encouraging in the case of the AERONET Cimel reference even when ignoring the cloud-screening algorithm of the other two direct sun-pointing instruments (the standard deviations between the wavelengths being in the order of 0.01 or less). Both the MBD and the RMSD between the Cimel and the PFR are substantially greater than those between the CIMEL and the SP01A. The standard deviation of the AOD differences at all compared wavelengths for the sun-pointing instruments is found to be <0.01, with the value <0.005 for the Cimel/SP01A pair. The AOD observations of the MFRSR instruments do not compare to the Cimel as well as the

Table 3. Mean Bias Difference, Root Mean Square Difference, and Standard Deviation Between Aerosol Optical Depths at GAW PFR Sun Photometer Wavelengths and the Corresponding Wavelengths of the SP01A and MFRSR Instruments[a]

Instrument	Wavelength, nm	All Data MBD	All Data RMSD	All Data σ	N	Clear MBD	Clear RMSD	Clear σ	N	Air Mass < 6 MBD	Air Mass < 6 RMSD	Air Mass < 6 σ	N
MSC SP01A	368	−0.0062	0.0106	0.0085	15594	−0.0058	0.0086	0.0063	12928	−0.0058	0.0076	0.0050	9795
	412	−0.0068	0.0071	0.0055	15765	−0.0063	0.0080	0.0049	13265	−0.0074	0.0087	0.0046	9807
	502	−0.0066	0.0077	0.0058	15805	−0.0064	0.0085	0.0055	13321	−0.0084	0.0091	0.0035	9808
	862	−0.0026	0.0079	0.0074	15634	−0.0026	0.0049	0.0041	13051	−0.0044	0.0053	0.0030	9900
USDA MFRSR	415	0.0022	0.0145	0.0144	5694					0.0004	0.0091	0.0091	4530
	500	0.0068	0.0142	0.0125	5827					0.0053	0.0121	0.0108	4538
	860	0.0076	0.0134	0.0110	5856					0.0076	0.0130	0.0106	4536
MSC MFRSR	415.8	−0.0052	0.0194	0.0187	17335					−0.0039	0.0123	0.0117	13657
	496.4	0.0061	0.0186	0.0175	17947					0.0012	0.0107	0.0107	13715
	869.5	0.0150	0.0208	0.0145	17761					0.0114	0.0142	0.0085	13712

[a]SP01A and MFRSR wavelengths are 367.8, 411.9, 500.4, and 862.9 nm.

Table 4. Mean Bias Difference, Root Mean Square Difference, and Standard Deviation Between Aerosol Optical Depths at MSC SP01A Sun Photometer Wavelengths and the Corresponding Wavelengths of the MFRSR Instruments[a]

Instrument	Wavelength, nm	All Data MBD	All Data RMSD	All Data σ	N	Air Mass < 6 MBD	Air Mass < 6 RMSD	Air Mass < 6 σ	N
USDA MFRSR	415	0.0114	0.0257	0.0231	5817	0.0122	0.0209	0.0169	4464
	500	0.0175	0.0251	0.0180	5880	0.0178	0.0244	0.0167	4663
	665	0.0101	0.0186	0.0157	5872	0.0099	0.0181	0.0152	4661
	860	0.0142	0.0232	0.0174	5803	0.0161	0.0240	0.0170	4604
MSC MFRSR	415.8	−0.0001	0.0345	0.0344	17961	0.0065	0.0227	0.0217	14164
	496.4	0.0153	0.0287	0.0243	17960	0.0119	0.0248	0.0218	14045
	671.6	0.0139	0.0264	0.0224	17958	0.0109	0.0242	0.0217	14162
	869.5	0.0200	0.0305	0.0229	17736	0.0185	0.0292	0.0226	13994

[a]MSC SP10A wavelengths are 412, 502, 675, and 862 nm.

sun-pointing instruments, but the standard deviation of the AOD differences at all wavelengths for both instruments remains well <0.02. The MBD and RMSD between the Cimel and the MFRSR are generally greater than twice that calculated for the sun-pointing instruments, possibly indicating the difficulty in calculating low AOD values from a differencing methodology that also depends on averaged data. The increase in the value of both the MBD and the RMSD may be attributed to the influence of cloud during the duration of the averaging period. However, if this were the sole reason for such differences, it would be expected that the MSC MFRSR would have performed significantly better than the USDA instrument because of the shorter averaging period. The larger discrepancy between these two types of instruments is probably due to the incorrect characterization of the directional responsivity of the instruments and the changing field of view with increasing air mass.

[43] The MBD and the RMSD for the MSC SP01A are found to be smaller than for the GAW PFR by approximately a factor of 2 before the cloud-screening algorithms of these two instruments are considered. When the data is examined following application of these cloud-screening algorithms, the results improve, but the number of observations is reduced substantially. A discussion of the discrepancies among cloud contamination algorithms follows. The agreement between the Cimel level 2.0 data and the cloud-screened data of the PFR and SP01A is excellent. With the exception of the Cimel/PFR 500-nm pair, the 2σ deviations are <0.01. This indicates that direct-pointing instruments with the appropriate cloud-screening techniques can provide data that meets the World Climate Research Programme BSRN AOD accuracy criterion of 0.01 [*World Climate Research Programme (WCRP)*, 1998]. However, the AOD values obtained from the two MFRSR instruments are in much poorer agreement, even considering the poten-

tial problems associated with cloud contamination. There are no cases where the RMSD is <0.01 and only one case where it is <0.02. The MBDs are also significantly greater than those associated with the direct-pointing instruments.

[44] Table 3 is a comparison of the remaining instruments against the GAW PFR. The results in the columns labeled "All Data" in Table 3 are based on the PFR cloud-screening algorithm. As each of these instruments begins taking measurements at sunrise, the initial comparison results use all the observations that have passed through the quality assurance procedures described earlier. The results are similar to those seen between the Cimel and the other instruments when only a single cloud-screening method is employed. The comparison of the 368-nm filters between the PFR and the SP01A show larger RMSD than at longer wavelengths, which in turn is reflected in the increased standard deviation over the other filters. This may indicate the increased variability that can be expected at shorter wavelengths because of differences in the methods used in calculating Rayleigh scatter and the differences associated with individual pressure observations versus daily averages. The second set of columns in Table 3 ("Clear") give the results for all zenith angles, but only when both the SP01A and the PFR algorithms indicate no cloud contamination. The difference in the number of observations flagged by only one cloud-screening algorithm, but not both between the PFR and the SP01A, is much smaller than in the case of the AERONET comparison. However, the discrepancy in the number of cloud-screened observations between the various methods remains significant. The RMSD between the GAW PFR and MSC SP01A is smaller than between the GAW PFR and the AERONET Cimel, as expected from the comparison of each of these instruments against the Cimel. The scatter is shown to have increased somewhat over the Cimel values when all data are considered. Nevertheless, the 2σ values for the 412- and 862-nm pairs remain below

Table 5. Mean Bias Difference, Root Mean Square Difference, and Standard Deviation Between Aerosol Optical Depths for the Two MFRSR Instruments With the USDA Instrument Considered the Reference Instrument[a]

Instrument	Wavelength, nm	Clear MBD	Clear RMSD	Clear σ	N	Air Mass < 6 MBD	Air Mass < 6 RMSD	Air Mass < 6 σ	N
MSC MFRSR	415.8	−0.0109	0.0226	0.0308	6509	−0.0068	0.0250	0.0240	5309
	496.4	−0.0038	0.0240	0.0237	6614	−0.0068	0.0226	0.0215	5300
	613.6	0.0039	0.0215	0.0212	6605	0.0016	0.0188	0.0186	5292
	671.6	0.0024	0.0223	0.0232	6637	0.0005	0.0189	0.0189	5297
	869.5	0.0050	0.0235	0.0229	6627	0.0023	0.0195	0.0193	5294

[a]Aerosol optical depths for the MFRSR instruments are 415, 500, 610, 665, and 860 nm. The removal of cloud contaminated data was based on the cloud-screened GAW PFR observations.

0.01, while the 368- and 500-nm pairs only slightly exceed this value.

[45] The results of the two MFRSR instruments are poorer than the direct-pointing instruments, but both MFRSR instruments are found to have smaller MBD with respect to the PFR than the Cimel when the evaluation is based on the complete PFR cloud-screened data set. The RMSDs are also found to be smaller for the USDA MFRSR. The MSC MFRSR RMSD values are marginally larger at the 500-nm wavelength and smaller at the 869-nm wavelength. The overall standard deviation is found to be smaller for the USDA MFRSR at the two comparable wavelengths of 500 and 860 nm when compared against the PFR over the Cimel instrument.

[46] To better compare the results obtained with the PFR as the reference instrument with those using the Cimel as the reference instrument, the statistics were recalculated for data that were collected at air mass values <6. The final four columns of Table 3 present these results. The data used in the comparison between the PFR and SP01A used are those that both algorithms indicated were free of cloud contamination. Again, the results of the comparison between the direct-pointing instruments are exceptionally good, with even the 368-nm channel having a standard deviation of only 0.005. This implied level of optical depth accuracy is particularly encouraging because of the increasingly significant role that the determination of Rayleigh optical depth plays at shorter wavelengths; a variation of 10-hPa pressure would result in a change in Rayleigh optical depth at 368 nm of 0.007 that would be directly attributed to the AOD. While the GAW PFR instrument includes an onboard pressure transducer, the MSC SP01A data have been calculated on the basis of a daily mean pressure, indicating that in the UV-A, pressure corrections may be crucial in obtaining the high-quality AOD observations required for monitoring climate variability (i.e., the pressure-induced uncertainty may be a major component of the 0.0076 value computed for 368 nm in Table 3). The statistics for the MFRSR instruments also improve dramatically when only values for air mass <6 are used in the analyses. The standard deviation about the AOD differences between the PFR and the MFRSR instruments are on the order of 0.01. This agreement is much better than between the Cimel and the MFRSR instruments, although the difference between the direct-pointing instruments versus the rotating shadowband instruments still differs by a factor of two.

[47] Table 4 compares the two MFRSR instruments against the MSC SP01A. The results of the comparison between the SP01A and the USDA MFRSR for air mass values <6 are similar to the results presented between the Cimel and the USDA MFRSR in Table 2. The MSC MFRSR results for air mass <6, however, are characterized by larger RMSD values than those calculated using either the Cimel or the PFR as the reference instrument.

[48] Table 5 completes the comparison of AOD values by presenting the differences between the two MFRSR instruments. The USDA instrument was selected as the reference. To overcome the problem associated with determining whether cloud was interfering with the measurements, the data used in the comparison was matched with the times the GAW PFR cloud-screening algorithm indicated clear line-of-sight conditions. Overall, for Air Mass <6 the standard deviation of AOD differences between the two instruments is found to be only marginally larger than between the individual MFRSR instruments and the three direct-pointing instruments.

5.2. Ångström Coefficients

[49] While the determination of Ångström coefficients is linear on a log-log scale and therefore very easy to calculate, the actual optical depth spectrum is typically characterized by nonlinear spectral curvature in the optical domain [*O'Neill et al.*, 2001] and is sensitive to the wavelength range used in the determination of the coefficients [*Cachorro et al.*, 2001]. Although these considerations would indicate that comparing Ångström values may be error prone, many aerosol networks produce the α exponent as a prime indicator of the aerosol character. It has also been used to interpolate AOD values for unknown wavelengths in comparisons [*Schmid et al.*, 1999] and climatologies [*Holben et al.*, 2001], indicating its importance in aerosol observation science. Therefore comparison between network values is inevitable.

[50] The atmospheric aerosols encountered over the BLO are continental in nature, well aged, and distant from point sources. These characteristics are similar to those associated with the original use of Ångström's coefficients for determining aerosol optical properties for visible wavelengths [*Junge*, 1963].

[51] The algorithms associated with the three direct-pointing instruments calculate the α coefficient for each observation. The comparability of these values provides both an overall assessment of the similarity of the AOD values at all wavelengths measured by each instrument and an independent measure of the confidence that can be placed on the more complex radiative properties derived from the instruments through various inversion techniques [e.g., *Dubovik et al.*, 2000]. The MBD and RMSD between the computations obtained from the three instruments are given in Table 6. The mean α value in Table 6 is calculated as the average of both sets of observations and is provided to assist in assessing the quality of the agreement among the various instruments. The calculations followed the same selection methodology as used in determining the AOD results. It is readily apparent that the agreement between the GAW PFR and the MSC SP01A is significantly better than between those instruments and the AERONET Cimel. The larger MBD and RMSD values associated with the AERONET Cimel were found to be surprising considering the general good agreement between the aerosol optical depths at the compared wavelengths. The calculations of MBD and RMSD were repeated using the AERONET reported α calculated using the full Cimel wavelength set, but no improvement was found.

[52] The differences between the calculated α are a function of the uncertainty associated with the determination of α from individual instrument AODs, which is related to the uncertainty in the determination of the AODs and the quality of the calculation of α and the uncertainty due to the differences in the AOD values between instruments. To determine the uncertainty associated with individual α, the Ångström coefficients were recalculated so that the standard deviation about the regression equation

Table 6. Mean Bias Difference and Root Mean Square Difference of the Ångström α Exponent Calculated From Instantaneous Aerosol Optical Depth Measurements From the AERONET Cimel, GAW PFR, and MSC SP01A Photometers[a]

Instrument Pair	Mean α	MBD	RMSD
GAW PFR and MSC SP01A	1.4608	−0.0244	0.0816
AERONET Cimel and GAW PFR	1.5387	0.1882	0.2601
AERONET Cimel and MSC SP01A	1.556	0.1598	0.2467

[a]The wavelengths used in the calculations are the following: Cimel, 437, 498, 669, and 871 nm; PFR, 367.8, 411.9, 500.4, and 862.9 nm; SP01A, 368, 412, 502, 675, 778, and 862 nm.

(s) could be determined as a measure of the uncertainty associated with an individual α. While the results of the calculations are not exact, owing to rounding errors between the original data and the truncated published data, the difference between these coefficients is on the order of 10^{-3}. Figure 7a plots α as a function of δ_{500} for clear-sky observations of the three direct-pointing instruments, while Figure 7b graphs s for each instrument in a similar manner. Figure 7c shows $\Delta\alpha$ as a function of δ_{500}. Figure 7d illustrates an uncertainty term associated with s and the differences between the AODs at compared wavelengths. This latter term, denoted by Ψ, attempts to explain both the uncertainty due to the regression associated with the computation of α for both instruments and the uncertainty between instruments due to differences in the measurement of the respective δ_λ, in the form

$$\Psi = \left[s_1^2 + s_2^2 + \sum_n \Delta\delta_{\lambda_{1,2}}^2 n^{-1} N\right]^{0.5}, \quad (9)$$

where s_1 and s_2 are the standard deviation of the regression from instruments 1 and 2. $\Delta\delta_\lambda$ is the difference in the natural logarithms of AOD for wavelength λ (to be comparable to the evaluation of the standard deviations associated with calculation of α), n represents the number of comparable channels for the two instruments being compared, and N is the total number of channels of the reference instrument. This term does not fully represent the uncertainty associated with $\Delta\alpha$ because the uncertainty associated with the determination of AOD by the various network methods has not been included explicitly, and only the differences in the AODs at compared wavelengths are known. An attempt has been made to normalize this latter uncertainty between instrument pairs by assuming that the mean difference of the compared wavelengths approximates the mean differences if all wavelengths could be compared.

[53] The large uncertainties associated with the calculation of α at low AOD indicate that the large differences between α values for the different instruments should not be surprising. The uncertainty at low AOD is dominated by the uncertainty associated with the differences in the calculated AOD. By contrast, with $\delta_{500} > 0.15$ the differences between the PFR and the SP01A values are approximately ±1–2%, with the uncertainty being dominated by the standard deviations about the regressions used to calculate α. During the comparison period the mean clear sky δ_{500} was <0.1 with the median value being 0.074. This suggests that extreme caution should be exercised in comparing aerosol

optical characteristics derived from low optical depths [*O'Neill et al.*, 2002].

[54] A second determination of Ångström's coefficients was made on the basis of 18 half-day periods where the aerosol optical depth remained relatively constant for the
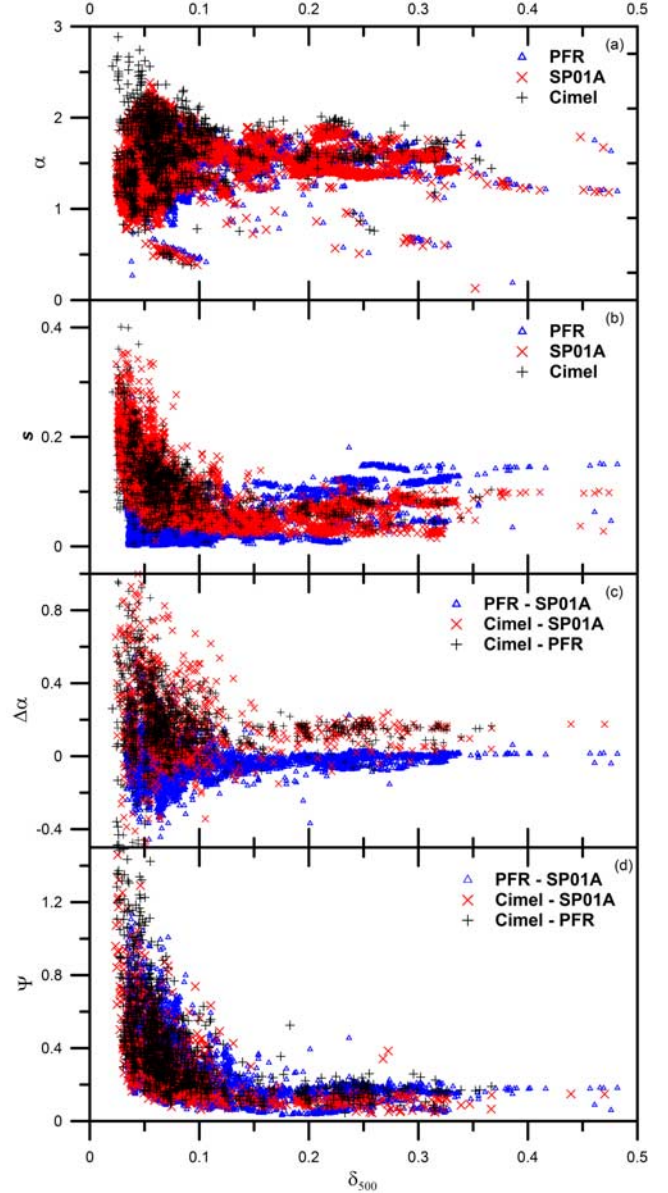
Figure 7. Plots relating the uncertainty associated with the calculation of the Ångström α with the uncertainty of the linear regression model used to calculate α and the differences between observed AODs. (a) The relationship between Ångström α as computed from individual observation sets from the three direct-pointing instruments with δ_{500} for the same instrument. (b) The standard deviation (s) about α. (c) The differences between α computed from various instrument pairs. (d) Ψ (see text) that combines the uncertainty associated with the standard deviation about the regression and the differences in AOD determinations by different instruments as a means of understanding the observed discrepancies between network evaluations of α.

entire period. The mean AOD for each wavelength from all five instruments was determined over the air mass range of 2−6. These data were then used to obtain the α coefficients for the period (Figure 8). The results confirm the discrepancies between the AERONET Cimel, GAW PFR, and MSC SP01A results reported above. In all cases the α determined from the AERONET Cimel data is larger than those calculated using data from the other photometers in the comparison. The MFRSR results in this graph indicate that the MSC instrument significantly underestimates α for all periods. This corresponds to the significant and generally increasing bias with wavelength between the MSC instrument and the direct-pointing instruments (Tables 2−4) that is indicative of a spectral flattening compared to the other instruments. The USDA MFRSR results suggest a solar position dependency, the morning values being smaller than the α calculated from both the GAW PFR and MSC SP01A data, with the afternoon values being greater or nearly equal. The rapid increase in AOD near midday exhibited by this instrument (Figure 2) occurs at air mass values <2 and so does not enter into these calculations. The large range in α seen in Figure 8 indicates the magnitude of the uncertainties that may exist between Ångström coefficients derived from the various network instruments. These results would indicate that using such parameters, as part of a global climatology, should be discouraged at present.

5.3. Cloud Screening Algorithms

[55] The AOD observations that have been used in this comparison are based on automatic cloud-screening techniques. The discrepancies in the number of observations that were removed because of apparent cloud contamination by the different quality assurance procedures were found to be greater than anticipated. Therefore a brief analysis has been undertaken to determine the differences between the methods. Unfortunately, continuous cloud observations are not made at present at the BLO, so no definitive conclusion can be made as to the overall quality of the screening algorithms. However, it is believed that comparing the differences between the instruments will encourage more effort in testing the present approaches and the development of new algorithms.

[56] The AERONET data are both prescreened for data quality at the time of the observation and screened during an automatic quality control procedure. Neither the GAW PFR nor the MSC SP01A data are prescreened, but both use automatic quality assurance procedures that indicate whether cloud is present during the observation. In both cases the flagged data remain as part of the data set. Details of the screening procedures are given in section 3. Before the cloud-screening algorithms were compared, any data associated with instrument malfunctions or pointing errors were removed. For the AERONET data it was assumed that all observations removed between level 1.0, unscreened data and level 1.5 cloud-screened data were due only to the cloud-screening process and that the difference in the number of observations between level 1.5 data and the level 2.0 data used in the comparison were for reasons other than cloud contamination. The slight differences in the times of matched observations are not expected to alter the overall results of the comparison. It is recognized that on days where observations were made during conditions of scattered
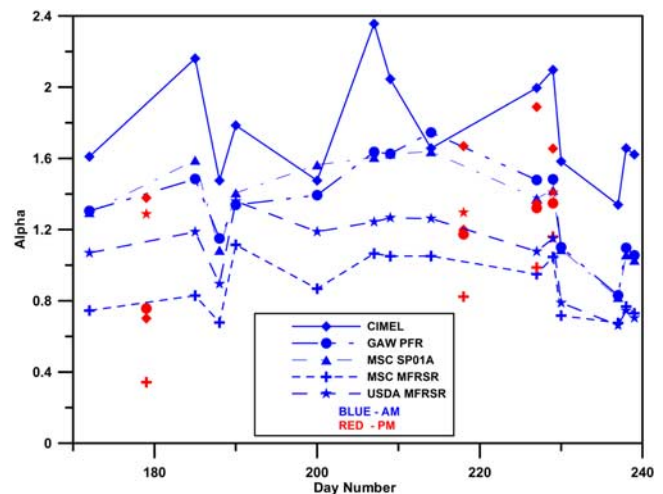
Figure 8. Comparison of the Ångström Alpha exponent calculated from half-day mean AODs calculated by the five network instruments.

clouds, individual observations among the three might show differences, but it is expected that the randomness of this process will not result in significantly different numbers of screened observations overall.

[57] Between 11 June and 28 August the AERONET Cimel reported 2782 valid level 1.0 observations (level 1.0 less the difference between level 1.5 and level 2.0 observations), of which 67% were determined to be cloud-free by the AERONET cloud-screening algorithm (Table 7). During the same period the GAW algorithm screened out 69% of its observations as cloud contaminated and the MSC algorithm screened out 49% of all observations as contaminated by cloud. AERONET employs a ''coarse triplet rejection'' criterion on three observations taken 30 s apart over a 1-min period, and data not passing the test are not transmitted. As the number of AERONET Cimel observations not reported because of this is unknown, the pre-cloud-screened data from the GAW and MSC data sets were paired with the valid Cimel level 1.0 data to permit a similar reference for determining the percentage of cloud-free data. In contrast to the general percentages of data rejected as cloud contaminated, the GAW algorithm applied to the PFR observations obtained at the same time as the AERONET Cimel level 1.0 observations, determined only 51% to be cloud-free, 16% less than the AERONET algorithm resolved. Not only is there a significant difference in the number of observations that were determined to be uncontaminated by cloud, but there is also a discrepancy between which observations were determined to be cloud contaminated. As the comparison between the AERONET algorithm and the algorithms used for the PFR and SP01A is based on the level 1.0 and above data, the issue of offset time is eliminated because observations were obtained within the period of the Cimel triplet observation. Using the GAW rejection criteria, 42% of the AERONET level 2.0 data would have been determined to be cloud contaminated. This does not imply, however, that the GAW algorithm is simply more conservative in its determination of cloudless conditions. Approximately 12% of the Cimel level 1.0 temporally matched data were determined to be cloud

Table 7. Comparison of Cloud-Screening Algorithms Based on the Percentage of Valid Observations[a]

Cloud-screening Algorithms	Number of Observations	AERONET Cloudless, %	GAW Cloudless, %	MSC Cloudless, %	Both Cloudless, %	First Cloudless, Second Cloudy, %	First Cloudy, Second Cloudless, %
AERONET	2782	67.3					
GAW	58531		30.8				
MSC	37412			50.3			
AERONET and GAW	2614	66.4	50.9		38.5	27.9	12.5
AERONET and MSC	2226	69.6		58.6	44.4	25.2	14.2
GAW and MSC	35115		45.1	51.1	38.7	7.1	13.2

[a]The first three rows indicate the percentage of cloudless data based on the network algorithms for all valid observations obtained by the network instrument. The last three rows indicate the percentage of cloudless data determined by each algorithm for comparable sets of observations. The last three columns indicate the fraction of the total number of observations when (1) both algorithms indicated cloudless conditions, (2) the first algorithm indicated that the observation was cloudless but the second algorithm flagged the observation as cloud contaminated, and (3) the first algorithm indicated the observation was contaminated by cloud but the second algorithm processed it as cloudless.

contaminated by the AERONET algorithm but were classified as clear by the GAW algorithm.

[58] In comparing the GAW and MSC cloud-screening algorithms the sample size for temporally matched data is significantly larger, being >35,000 observations. The GAW algorithm flagged 55% of the data as cloud contaminated, and the MSC algorithm indicated that 49% was contaminated by cloud. Of the cloudless data, as determined by the MSC algorithm, the GAW screening method indicated that 26% was cloud contaminated. Conversely, the MSC algorithm claimed only 16% of the GAW-screened data was cloud contaminated.

[59] These results must be considered with a certain amount of caution. The mandate of the GAW is to observe background aerosols in remote locations. The conservative nature of the cloud contamination scheme may serve this purpose well. The AERONET and MSC schemes, however, are to screen out cloud contamination that would hinder the determination of aerosol climatology and trends. Too conservative a screening may well eliminate data from local events that should be part of the aerosol record, while screening that does not readily sense cloud contamination will introduce biases associated with thin uniform cloud such as cirrus.

6. Conclusions

[60] A comparison of network instruments routinely used to measure aerosol optical depths both regionally and globally occurred during the summer of 2001 at the Bratt's Lake Observatory (Saskatchewan, Canada). Three direct-pointing photometers and two Multifilter Rotating Shadowband Radiometers were operated continuously for the comparison. The instruments were monitored following normal protocols. The data were either provided by the network administrator or calculated in the manner prescribed by the network depending on the location at which the data were stored.

[61] The results indicate that the three pointing instruments provide data of comparable quality. On an observation-by-observation basis the direct-pointing instruments appear to maintain a difference of <0.01 (2σ) for nearly all wavelengths in clear stable conditions. These results compare well with the uncertainty estimates presented to the BSRN at the Sixth BSRN Science and Review Workshop and adopted as the level to be achieved at all network locations observing AODs [WCRP, 2001]. It is estimated

that improvements in pointing; better determination of the effects of Rayleigh, ozone, and other absorbers on the calculation of aerosol optical depth; and better instrument characterization, including calibration of the radiometers, may improve agreement at the 0.005 level. Significant improvements in optical depth precision and interinstrument accuracy were obtained upon application of cloud-screening algorithms. Another, well-defined comparison of these instruments that includes an accurate and independent means of determining a cloud-free line of sight is essential.

[62] The MFRSR results for small aerosol optical depths were poorer than for the direct-pointing instruments. Better overall angular characterization of these instruments is probably necessary if they are to be used in monitoring background aerosol optical depths. The two instruments, although obtained from the same manufacturer, were characterized at different laboratories and were calibrated using different methods. Neither instrument showed significant superiority over the other. The RMSD between the two instruments was found to be nearly as large as the magnitude of the optical depths that were being measured. These comparisons indicate that the MFRSR cannot match the precision and accuracy of the direct sun-pointing instruments for AOD measurements for clean atmospheres with values of ≤0.1. Until the problems associated with this type of instrument are understood fully and corrected, they cannot be recommended for the measurement of aerosol HTML file characteristics at background or rural locations.

References

Ångström, A., On the atmospheric transmission of Sun radiation and on dust in the air, *Geogr. Ann., 11,* 156–166, 1929.

Bass, A. M., and R. J. Paur, The ultraviolet cross-sections of ozone, in *The Measurements in Stratospheric Ozone*, edited by C. S. Zerefos and A. Ghazi, pp. 606–610, D. Reidel, Norwell, Mass., 1985.

Bigelow, D. S., J. R. Slusser, A. F. Beaubien, and J. H. Gibson, The USDA Ultraviolet radiation monitoring program, *Bull. Am. Meteorol. Soc., 79,* 601–615, 1998.

Bodhaine, B. A., N. B. Wood, E. G. Dutton, and J. R. Slusser, On Rayleigh optical depth calculations, *J. Atmos. Tech., 16,* 1854–1861, 1999.

Bokoye, A. I., A. Royer, N. T. O'Neill, G. Fedosjevs, P. M. Teillet, and B. McArthur, Characterization of atmospheric aerosols across Canada from a ground-based Sunphotometer network: AEROCAN, *Atmos. Ocean, 39*(4), 429–456, 2001.

Bucholtz, A., Rayleigh-scattering calculations for the terrestrial atmosphere, *Appl. Opt., 34,* 2765–2773, 1995.

Burrows, J. P., A. Richter, A. Dern, B. Deters, S. Himmelmann, S. Voight, and J. Orphal, Atmospheric remote-sensing reference data from GOME: Part 2. Temperature dependent absorption cross-sections of O3 in the 231–794 nm range, *J. Quant. Spectrosc. Radiat. Transfer*, *61*, 509–517, 1999.

Cachorro, V. E., R. Vergaz, and A. M. de Frutos, A quantitative comparison of α-Å turbidity parameter retrieved in different spectral ranges based on spectroradiometer solar radiation measurements, *Atmos. Environ.*, *35*, 5117–5124, 2001.

Chance, K., and R. J. D. Spurr, Ring effect studies: Rayleigh scattering, including molecular parameters for rotational Raman scattering, and the Fraunhofer spectrum, *Appl. Opt.*, *36*, 5224–5230, 1997.

Dubovik, O., A. Smirnov, B. N. Holben, M. D. King, Y. J. Kaufman, T. F. Eck, and I. Slutsker, Accuracy assessments of aerosol optical properties retrieved from Aerosol Robotic Network (AERONET) Sun and sky radiance measurements, *J. Geophys. Res.*, *105*, 9791–9806, 2000.

Eck, T. F., B. N. Holben, J. S. Reid, O. Dubovik, A. Smirnov, N. T. O'Neill, I. Slutsker, and S. Kinne, Wavelength dependence of the optical depth of biomass burning, urban, and desert dust aerosols, *J. Geophys. Res.*, *104*, 31,333–31,349, 1999.

Fedosejevs, G., N. T. O'Neill, A. Royer, P. M. Teillet, A. I. Bokoye, and B. McArthur, Aerosol optical depth for atmospheric correction of AVHRR composite data, *Can. J. Remote Sens.*, *26*, 273–284, 2000.

Forgan, B. W., Sun photometer calibration by the ratio-Langley method, in *Baseline Atmospheric Program (Australia) 1986*, edited by B. W. Forgan and P. J. Fraser, pp. 22–26, Bur. of Meteorol., Melbourne, Australia, 1988.

Forgan, B. W., General method for calibration sun photometers, *Appl. Opt.*, *33*, 4841–4850, 1994.

Gueymard, C., SMARTS2, a simple model of the atmospheric radiative transfer of sunshine: Algorithms and performance assessment, *Rep. FSEC-PF-270-95*, Fla. Sol. Energy Cent., Cocoa, Florida, 1995.

Harrison, L., and J. Michalsky, Objective algorithms for the retrieval of optical depths from ground-based measurements, *Appl. Opt.*, *33*, 5126–5132, 1994.

Harrison, L., J. Michalsky, and J. Berndt, Automated multifilter rotating shadow-band radiometer: An instrument for optical depth and radiation measurements, *Appl. Opt.*, *33*, 5118–5125, 1994.

Holben, B. N., et al., AERONET—A federated instrument network and data archive for aerosol characterization, *Remote Sens. Environ.*, *66*, 1–16, 1998.

Holben, B. N., et al., An emerging ground-based aerosol Climatology: Aerosol optical depth from AERONET, *J. Geophys. Res.*, *106*, 12,067–12,097, 2001.

Ingold, T., C. Mätzler, N. Kämpfer, and A. Heimo, Aerosol optical depth measurements by means of a Sun photometer network in Switzerland, *J. Geophys. Res.*, *106*, 27,537–27,554, 2001.

Junge, C. E., *Air Chemistry and Radioactivity*, Academic, San Diego, Calif., 1963.

Kasten, F., A new talbe and approximation formula for relative optical air mass, *Arch. Meteorol. Geophys. Bioklimatol., Ser. B*, *14*, 206–223, 1966.

Kasten, F., and A. T. Young, Revised optical air mass tables and approximation formula, *Appl. Opt.*, *28*, 4735–4738, 1989.

Kerr, J. B., and C. T. McElroy, Evidence for large upward trends of ultraviolet-B radiation linked to ozone depletion, *Science*, *262*, 1032–1034, 1993.

Komhyr, W. D., Operations Handbook—Ozone observations with a Dobson Spectrometer, *WMO Global Ozone Res. and Monit. Proj. No. 6.*, Natl. Ocean. and Atmos. Admin., Environ. Res. Lab., Air Resour. Lab., Boulder, Colo., 1980.

London, J., R. D. Bojkov, S. Oltmans, and J. I. Kelley, Atlas of the Global Distribution of Total Ozone July 1957–June 1967, *NCAR Tech. Note 133+STR*, 276 pp., Natl. Cent. for Atmos. Res., Boulder, Colo., 1976.

Michalsky, J. J., R. Perez, and R. Stewart, Design and development of a rotating shadowband radiometer solar radiation/daylight network, *Sol. Energy*, *6*, 577–581, 1988.

Michalsky, J. J., J. A. Schlemmer, W. E. Berkheiser, J. L. Berndt, L. C. Harrison, N. S. Laulainen, N. R. Larson, and J. C. Barnard, Multiyear measurements of aerosol optical depth in the Atmospheric Radiation Measurement and Quantitative Links programs, *J. Geophys. Res.*, *106*, 12,099–12,107, 2001.

Mitchell, R. M., and B. W. Forgan, Aerosol measurement in the Australian Outback: Intercomparison of Sun photometers, *J. Atmos. Oceanic Technol.*, *20*, 54–66, 2003.

O'Neill, N. T., T. F. Eck, B. N. Holben, A. Smirnov, O. Dubovik, and A. Royer, Bi-modal size distribution influences on the variation of Angstrom derivatives in spectral and optical depth space, *J. Geophys. Res.*, *106*, 9787–9806, 2001.

O'Neill, N. T., T. F. Eck, B. N. Holben, A. Smirnov, A. Royer, and Z. Li, Optical properties of boreal forest fire smoke derived from Sun photometry, *J. Geophys. Res.*, *107*(D11), 4125, doi:10.1029/2001JD000877, 2002.

Schmid, B., J. Michalsky, R. Halthorne, M. Beauharnois, L. Harrison, J. Livingston, P. Russell, B. Holben, T. Eck, and A. Smirnov, Comparison of aerosol optical depth from four solar radiometers during the fall 1997 ARM intensive observation period, *Geophys. Res. Lett.*, *26*(17), 2725–2728, 1999.

Shettle, E. P., and S. M. Anderson, New visible and near IR ozone absorption cross-sections for MODTRAN, in *Proc. 17th Annu. Rev. Conf. Atmos. Trans. Models, 8–9 June 1994, PL-TR-95-2060 Special Reports*, no. 274, edited by G. P. Anderson, R. H. Picard, and J. H. Chetwind, pp. 335–350, Phillips Lab., Directorate of Geophys., Hanscom Air Force Base, Mass., 1995.

Smirnov, A., B. N. Holben, T. F. Eck, O. Dubovik, and I. Slutsker, Cloud-screening and quality control algorithms for the AERONET database, *Remote Sens. Environ.*, *73*, 337–349, 2000.

Stephens, G. L., *Remote Sensing of the Lower Atmosphere*, Oxford Univ. Press, New York, 1994.

Vigroux, E., Contribution à l'etude experimentale de l'absorption de l'ozone, *Ann. Phys.*, *8*, 709, 1953.

Wehrli, C., Calibrations of filter radiometers for determination of atmospheric optical depth, *Metrologia*, *37*, 419–422, 2000.

World Climate Research Programme (WCRP), Report of the fifth BSRN science and review workshop, World Climate Research Programme Baseline Surface Radiation Network (BSRN), Budapest, Hungary, 18–22 May 1998, *WCRP Informal Rep. 10/1998*, Geneva, Switzerland, 1998.

WCRP, Report of the sixth BSRN science and review workshop, World Climate Research Programme Baseline Surface Radiation Network (BSRN), Melbourne, Australia, 1–5 May 2000, *WCRP Informal Rep. 17/2001*, Geneva, Switzerland, 2001.

————————————

D. H. Halliwell and O. J. Niebergall, Bratt's Lake Observatory, Meteorological Service of Canada, P.O. Box 160, Wilcox, Saskatchewan, Canada, S0G 5E0. (david.halliwell@ec.gc.ca; ojn_adair@sk.sympatico.ca)

L. J. B. McArthur, Meteorological Service of Canada, 4905 Dufferin Street, Downsview, Ontario, Canada M3H 5T4. (bruce.mcarthur@ec.gc.ca)

N. T. O'Neill, Le Centre d'applications et de recherches en télédétection, Univeristy of Sherbrooke, Sherbrooke, Quebec, Canada J1K 2R1. (noneill@courrier.usherb.ca)

J. R. Slusser, U.S. Department of Agriculture UV-B Monitoring and Research Program, Colorado State University, Fort Collins, CO 80523-1499, USA. (sluss@uvb.nrel.colostate.edu)

C. Wehrli, Physikalisch-Meteorologisches Observatorium/World Radiation Centre, 33, CH-7260 Davos, Switzerland. (chwehrli@pmodwrc.ch)